The relation between dynamics and activity of phospholipase A/acyltransferase homologs

Chatterjee, S.D.

3

Chapter

Molecular dynamics simulations reveal loop rearrangements in PLAAT4.

This chapter is based on joint work with Rubin Dasgupta

The work in this chapter was published as: Chatterjee, S. D., Zhou, J., Dasgupta, R., Cramer-Blok, A., Timmer, M., van der Stelt, M., and Ubbink, M. (2021) Protein Dynamics Influence the Enzymatic Activity of Phospholipase A/Acyltransferases 3 and 4. Biochemistry 60, 1178–1190.

Abstract

Molecular dynamics simulations are becoming increasingly commonplace to complement findings from NMR spectroscopy to study protein dynamics. In this study, we took a closer look at the dynamics of PLAAT3 and PLAAT4 to complement the knowledge obtained from NMR dynamics experiments. MD simulations support our earlier findings that PLAAT4 is inherently more flexible than PLAAT3. The active site of PLAAT4 is more mobile, in line with the observation that the resonances of many nuclei are missing in the ^{15}N-^{1}H HSQC spectrum due to exchange effects. An instability of the catalytic triad followed by a conformational rearrangement of L2(B6) in PLAAT4 was observed. The increased dynamics of this loop may relate to the higher activity of PLAAT4.

Introduction

To understand structure-function relationships of proteins, not only the ground state structures but also their dynamic properties need to be studied.[1,2] Protein dynamics occur at many timescales (Figure 3.1) and are linked to specific events such as bond vibrations (femtosecond timescale), side-chain rotations and loop motions (pico-nanosecond timescale) and biologically crucial processes such as folding, ligand binding and catalysis (micro-millisecond timescale).[3] Various spectroscopic techniques, including NMR spectroscopy and computational approaches such as molecular dynamics (MD) simulations, are used to study such motions to provide insight into the function of proteins. While NMR spectroscopy is an experimental technique that allows us to study fast (ns-ps) and slow motions (µs-ms) of a protein, it does not provide us with direct structural insights. MD simulations are used to study regions of protein, such as loops, that are flexible on a faster timescale and the technique provide us with direct structural insights. These loop regions can be crucial in protein-protein and protein-ligand interactions.[4,5] MD simulations are therefore often used to complement the findings from fast-timescale dynamics experiments (T_1, T_2 and cross relaxation parameters). NMR derived parameters, such as order parameters,[6,7] heteronuclear NOEs[8] and residual dipolar couplings[9] can be back-

calculated from MD simulations and compared with the experimental data to establish whether the simulation offers a good model for the true dynamics in a protein.

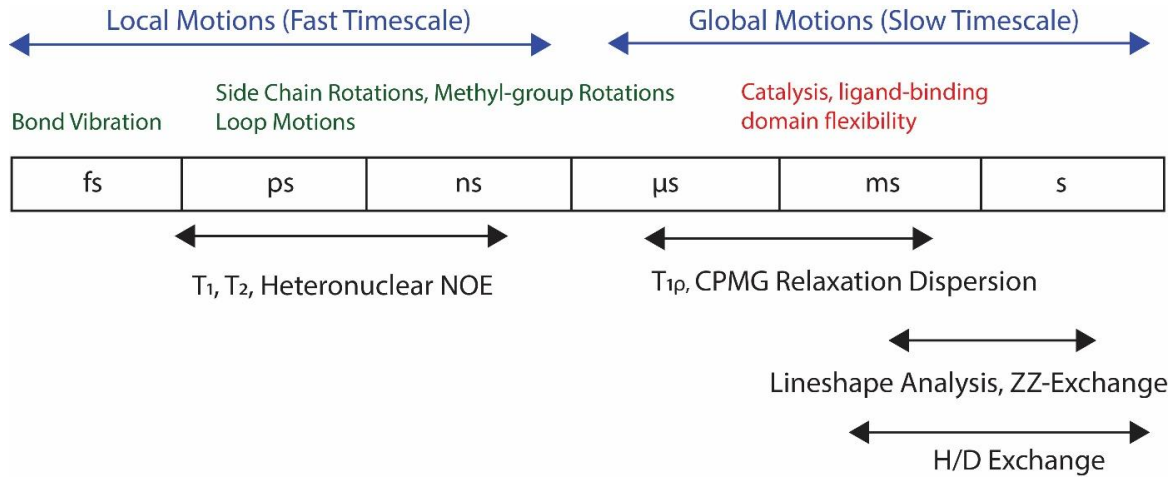

Figure 3.1 A graphical representation of different protein motions occurring at different timescales and their respective NMR experiments to study these motions. In protein dynamics, motions occurring at timescales below µs are termed as "fast timescale motions" whereas those occurring at timescales of µs or above are termed as "slow timescale motions".

MD simulations of proteins started to be used in the early 1980s.[10] Since then the technique has gained power enormously with the growth of computation power and parallelization techniques. The high-resolution information about exact position of an atom at any given time in the trajectory is one of the best features of this technique. However, the two major limitations of this technique are the length of the conformational sampling time and quality of the force-fields.[11]

In MD simulations, Newtonian equations of motions are solved for atoms taking into account interatomic forces. The parameters used to describe the forces between atoms are derived from various experimental and quantum mechanical calculations. Force fields take into account parameters for bond length, bond angles, torsion angles, van der Waals and electrostatic interactions.[12–15] Three things are essential for simulations, a starting structure (usually a pdb file), a force field, and a solvation model. A starting structure provides the atomic coordinates that can be obtained from experimental structures or homology models. The potential energy of the system in simulation is obtained from the force field, a parameterization of the energy surface of the protein. There are many different force field models and the most commonly used are the CHARMM,[16] AMBER,[17–19] and GROMOS[20,21] force fields. Frequently used

simulation software packages are CHARMM,[22] AMBER,[14] GROMACS,[23] and NAMD.[12] These packages share common capabilities and features but vary in their capacities, and underlying philosophies. The third important aspect of MD simulation is the choice of the solvent model, since the purpose for the simulation is to study protein motions under experimental conditions. The protein molecule is solvated using either of the two water models- the implicit or explicit solvent models. Implicit solvent does not take into account the movement of solvent molecules but rather averages the solvent conformations over its degrees of freedom.[24] The explicit solvent models allow the solvent molecules to be defined with a possibility of neutralising the system by adding counterions inside a solvent box. Various explicit solvent models exists such as TIP3P, TIP4P, TIP5P, SPC.[25–27]

A typical MD simulation starts with the energy minimization of the starting structure, followed by explicit solvation, the equilibration step and the final production step. In the equilibration step, the solvent molecules that were defined in case of explicit solvent models are allowed to move (equilibrate) by raising the temperature in small steps while protein positions are fixed. Equilibration steps are done under constant temperature and constant pressure conditions. In the production step the positional constraints on the protein are removed to let the protein and solvent to relax.

The trajectories are analysed to extract from the large data sets the information that is relevant for model building and comparison with experimental data. With modern processing units (CPUs, GPUs and supercomputing nodes) and efficient algorithms, large proteins or protein complexes can be simulated for 100s of ns and even µs. Analysis of the trajectories can be classified into four types: 1) Checking the integrity of the simulation and global analysis of the protein, including calculation of the root-mean-square deviation (RMSD) over time, the total energy of the system, the radius of gyration and the temperature and pressure fluctuations, 2) Cluster analysis by grouping the RMSD into separate conformational groups by k-means clustering or hierarchical approach,[28–30] 3) Principal component analysis to extract the correlated protein motions, also known as essential dynamics from sampled conformations,[31–34] and 4) Correlation function analysis of the bond-vectors to derive order parameters or atomic fluctuations to evaluate concerted motions in different parts of the protein.[35–37]

To complement the findings obtained from NMR dynamics studies of PLAAT3 and PLAAT4 (Chapter 2), we used MD simulations to study the internal motions of PLAAT3 and PLAAT4 to gain insights into the dynamics of the two proteins. In Chapter 2, we found contrasting

dynamics profile between the two proteins, especially for the flexible loop L1, residues around the active site and residues with nuclei missing resonance assignments in the NMR spectra, suggesting flexibility. Since the two proteins differ in phospholipase activity, MD simulations were performed to visualise protein dynamics to aid in our understanding of the two proteins. The results indicate significant differences between PLAAT3 and PLAAT4 active site dynamics, strengthening the findings from NMR experiments.

Results

Classical all-atom MD simulations on proteins were performed using NMR structures solvated in a rectangular water box, neutralized by counter ions and using the AMBER ff99sb-ILDN force-field. We used the GROMACS package, as it is open source, supports parallelization and GPU acceleration for faster non-bonded atomic calculations and possesses a large number of external tools for trajectory analysis.[38] Two runs of 100 ns were performed with different starting velocities for both PLAAT3 and PLAAT4.

Structural stability. The root mean-square deviation (RMSD) is an indicator of the global conformational stability of a structure during the simulation. Figure 3.2 presents the RMSD of the structural snapshots as compared to the starting structure over the course of the simulation. An initial jump in RMSD is normally observed within the first picosecond, which occurs due to the inherent fluctuation of atomic coordinates of the starting model as the spatial restrictions on the model are lifted. In the first 10 ns, the RMSD steadily increases as the protein samples different conformations. The RMSD value stabilizes after about 10 ns, with relatively minor fluctuations in the conformation. The larger RMSD observed for PLAAT4 indicates that considerable structural fluctuations are taking place over the course of the simulations. For example, in run 2 (seed 2), toward 70 ns, the RMSD increases further, suggesting that the protein undergoes a significant conformational rearrangement relative to the starting structure. In PLAAT3, the structure appears to remain relatively stable after the initial relaxation, suggesting that no significant structural fluctuations occur over the 100 ns period. The radii of gyration were also determined. They fluctuated around a value that remained stable during the MD simulations, with average values of 1.45 and 1.54 nm for PLAAT3 and PLAAT4, respectively (Figure 3.3).

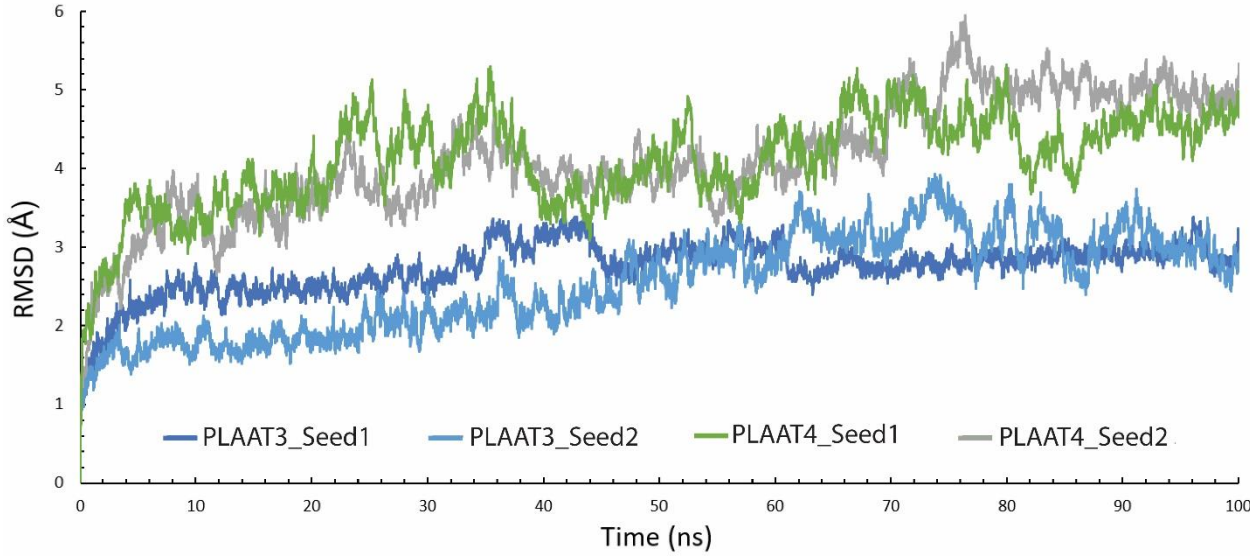

Figure 3.2 Plot of all atom RMSD of PLAAT3 and PLAAT4 runs. Each point in the frame represents a snapshot saved at every ps. PLAAT4 shows a higher RMSD, suggesting significant conformational fluctuations and rearrangements with respect to the starting structure.

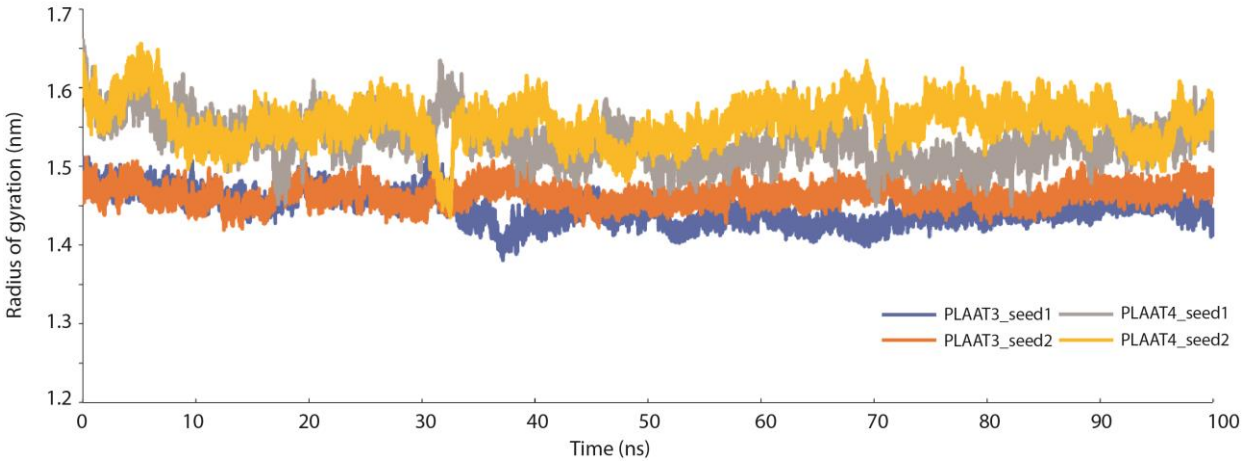

Figure 3.3. Plot of radius of gyration over the course of 100 ns MD trajectories in PLAAT3 and PLAAT4. For PLAAT3 and PLAAT4 the average Rgy values are 1.45 nm and 1.54 nm, respectively.

Essential dynamics. To observe and analyse important concerted motions (often known as essential dynamics), principal component analysis was performed. RMS fluctuations were calculated for all residues globally (Figure S3.1) and also for the top two eigenvectors (the two most significant principal components) to study essential dynamics (Figure 3.4). Residues with the highest RMS fluctuations of any atom above 2 Å were analysed and plotted on the NMR structures (Figure 3.5). In the course of the 100 ns simulations, it was observed that PLAAT3 maintains largely a rigid conformation, especially an ordered secondary structure. Apart from the disordered loop L1 (residues 43-55), only residues 19-22, along with 83-84 and the C-terminal residues 124-125 showed concerted flexibility. The distances between the active site atoms C113S_γ and H23N_δ and between H23N_ε and H35N_δ all remained below 5 Å (Figure S3.2), indicating that the active site triad (see Chapter 2, Figure 2.1.) remained intact.

In PLAAT4, more concerted motions were observed (Figure 3.4B). More residues in the flexible loop L1 (40-56), as well as residues 82-86, 88, 90, L2(B6) (108-111) and the N and C termini residues showed fluctuations above 2 Å, suggesting that these parts have correlated motions. In the active site of PLAAT4, C113S_γ exhibited an RMS fluctuation of 2.3 Å, while its backbone atoms were more rigid. This side-chain fluctuation came about as part of a significant rearrangement that took place in L2(B6). Since the α-helix A3, of which C113 is a part, is connected to this loop, its rearrangement rendered the active site quite mobile. The interaction between the cysteine of the catalytic triad and the histidine rings was disrupted during each of the two runs. Movements of the nucleophile residue C113S_γ and the base H23N_δ/N_ε and a concerted set of molecular rearrangements in the loop L2(B6) brought R111N_ε in close proximity of C113S_γ (Figure 3.6, panels A and B). The arginine side-chain was stabilized by the formation of two salt bridges with E114O_ε and E22O_ε. The interaction with the E114 was stable over almost the entire run. The distance between the side-chains of E22 and R111 showed some correlation with that between C113 and R111 (Figure 3.6, panels C and D). The interconversion between the active site in the native and disrupted active site states appears to happen fast and, thus, can be described by a two-state model, illustrated in Figure 3.7.

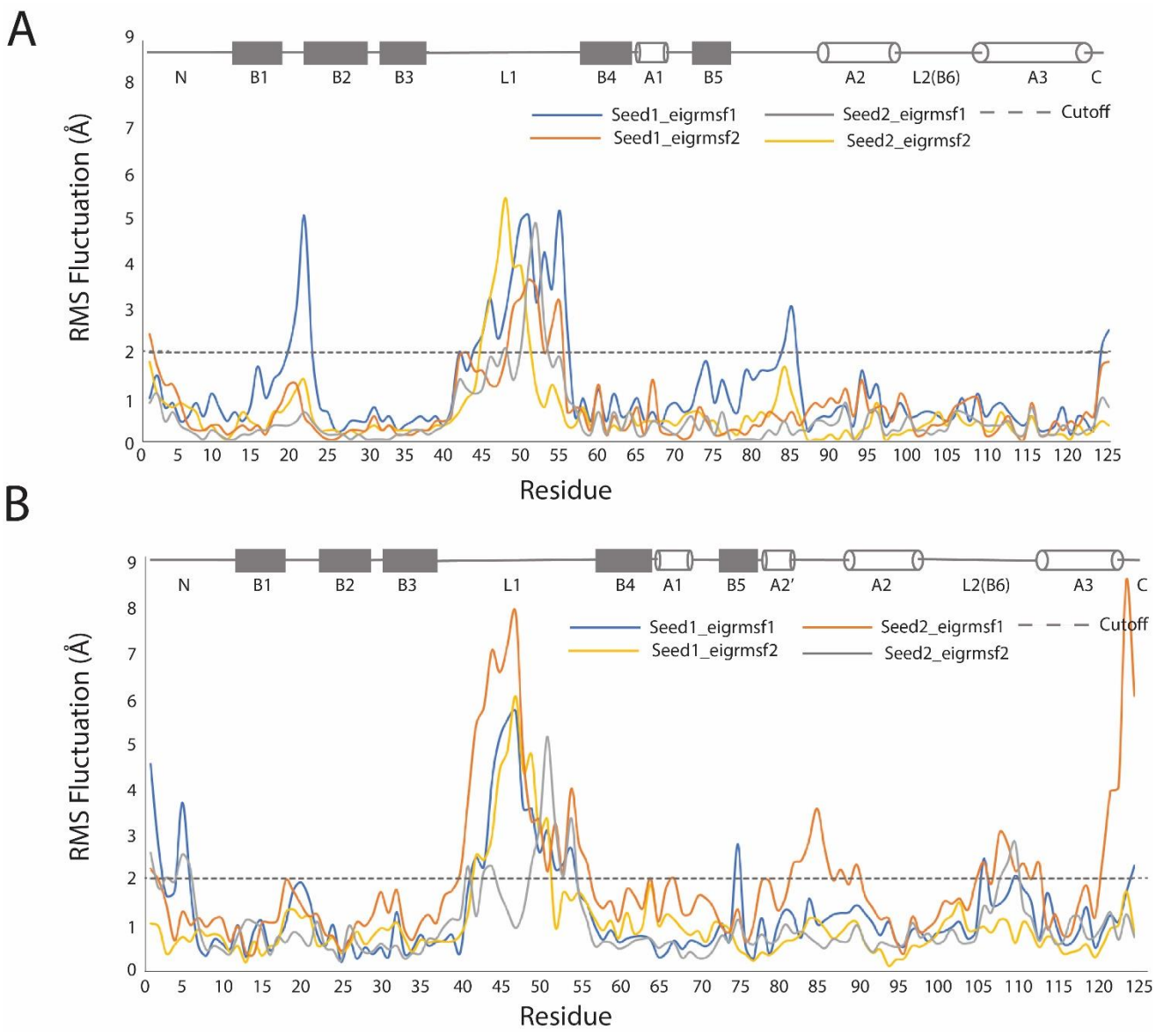

Figure 3.4 Fluctuations per residue. For each residue, the largest RMS fluctuation of all its atoms along the two largest eigenvectors of the principal components analysis in the MD runs is plotted for PLAAT3 (A) and PLAAT4 (B). A cut-off of 2 Å is indicated with a dashed line. Secondary structure of the starting structure is indicated at the top and named as per Table 2.1.

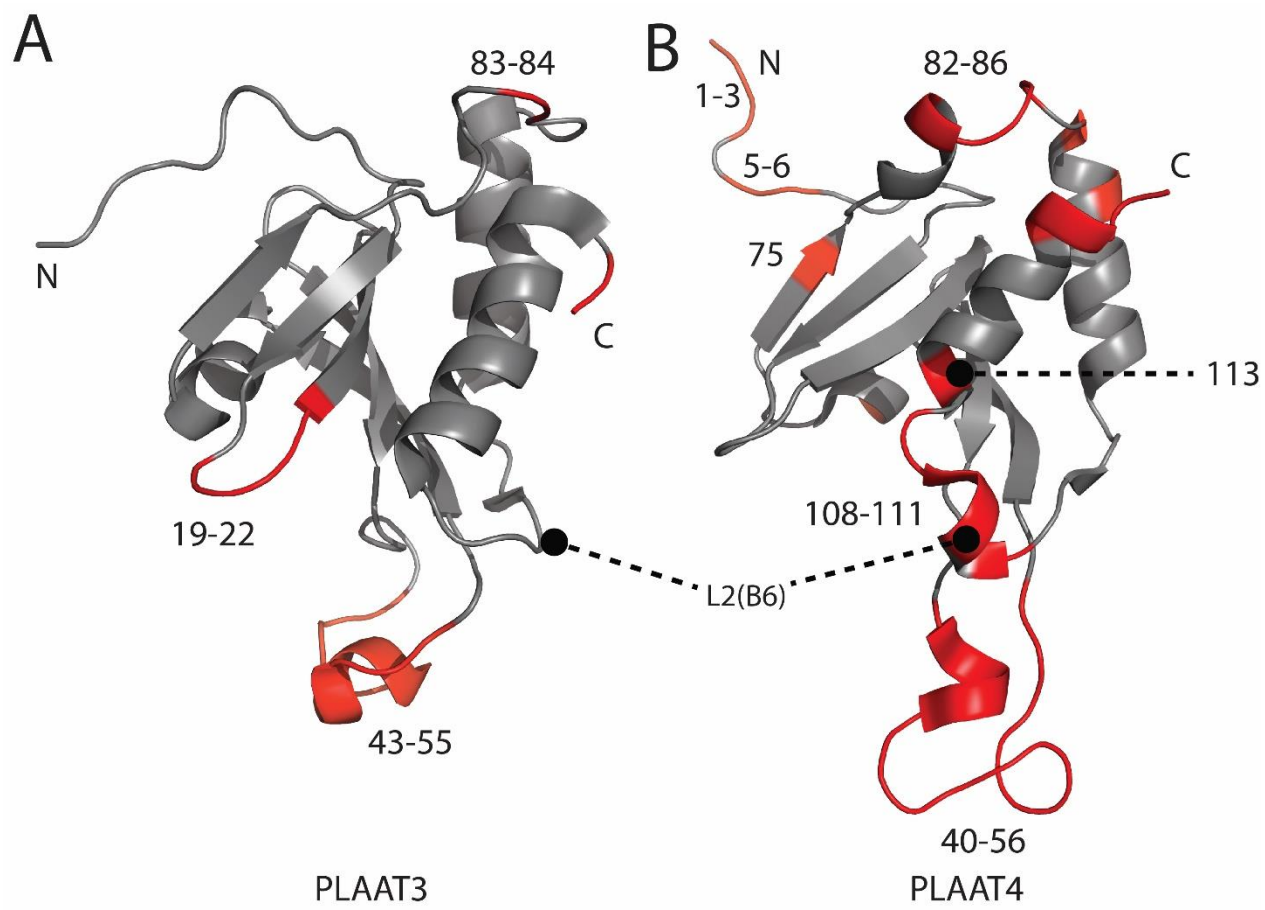

Figure 3.5 Results of principal component analysis of the MD simulations. Residues coloured in red in PLAAT3 (A) and PLAAT4 (B) show RMS fluctuations above the cut-off (Figure 3.4). Apart from the C terminus, two distinct regions in PLAAT3 (19-22 and 43-55) were observed having concerted motions, bringing them closer, while rest of the protein maintains relatively rigid. PLAAT4 has three distinct mobile regions apart from the N and the C termini. The flexible loop shows disordered movement while regions 108-111, 82-86 and residue 113 all show correlated motions, bringing the L2(B6) loop in close proximity to C113.

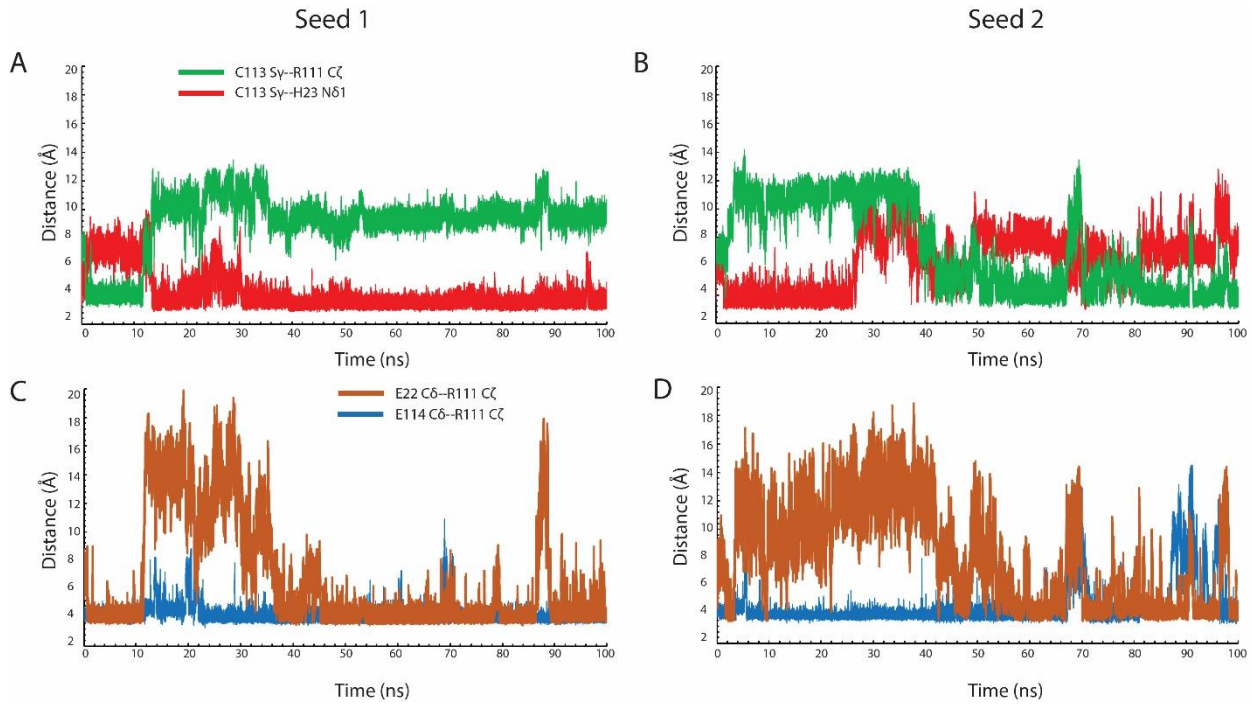

Figure 3.6 Inter-residue heavy atom distances during the two runs of MD simulations (seed 1 and seed 2). In PLAAT4 the distances between C113S_Y and H23$N_{\delta1}$ in PLAAT4 and that between C113S_Y and R111C_ζ are anti-correlated in both seed 1 (A) and seed2 (B) suggesting simultaneous disruption of the Cys-His-His catalytic triad interaction and formation of an interaction between R111 and C113. The distance between E114C_δ and R111C_ζ is around 4 Å throughout the simulation and the distance between R111C_ζ and E22C_δ is partially correlated to that between R111C_ζ and C113S_Y in both seed 1 (C) and seed 2 (D).

Discussion

Based on the observations obtained from both fast and slow timescale protein dynamics NMR experiments, as well as the MD simulations, a model is proposed for a two-state conformational rearrangement occurring in the catalytic region in PLAAT4, illustrated in Figure 3.7. In the starting structure the nucleophile residue C113 and the base residue H23 interact via a hydrogen bond. H23 is bound to H35, as part of the catalytic triad (panel A). The C113-H23 interaction can be broken and the imidazole rotates away. Simultaneously, L2(B6) and A3 rearrange, bringing the side-chains of R111 and C113 closer to form a new state. The observation of this mobility is in line with the experimental evidence for motion in this region. Nine out of 11 residues comprising L2(B6) in PLAAT4 either lack resonance assignments due to line broadening or show fast timescale dynamics. In PLAAT3 such dynamics is not observed.

Thus, these observations raise the question whether the mobility of L2(B6) relates to the activity difference between PLAAT3 and PLAAT4. Increased flexibility could play a role in substrate accessibility or induced fit. Since both PLAAT3 and PLAAT4 are membrane-anchored enzymes, a better substrate accessibility could lead to a higher (phospholipase) activity. To test this hypothesis, it would be interesting to test whether L2(B6) loop exchange between the two proteins would lead to different activities. Also interesting would be to study if this L2(B6) loop mobility affects native salt-bridge networks in PLAAT3 and PLAAT4 since salt bridges might infer protein rigidity/flexibility.[39,40] The findings are presented in chapter 4.

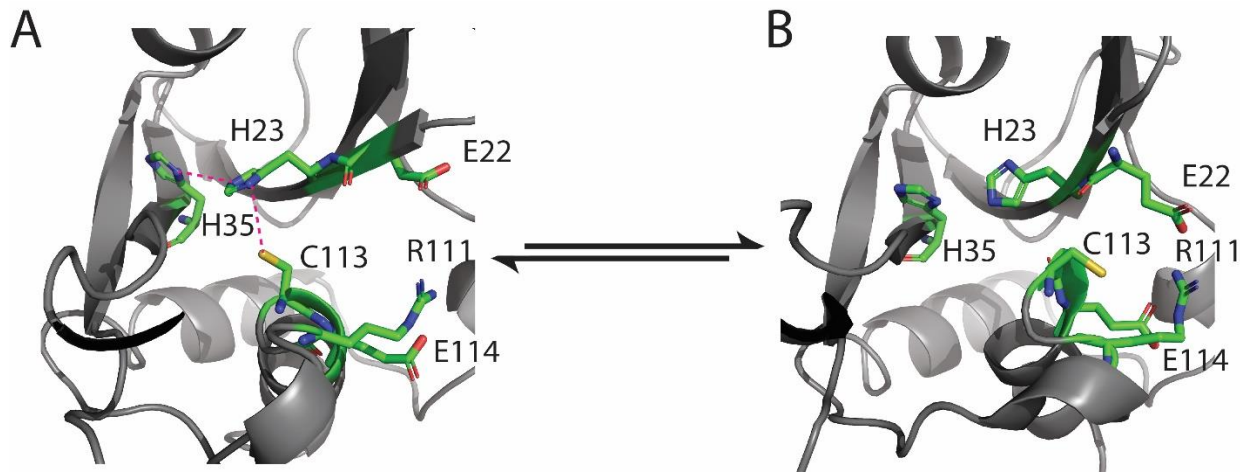

Figure 3.7 A model of the conformational rearrangements of PLAAT4 as described in the text. The Cys-His-His catalytic triad present in conformation A is disrupted in conformation B, in which C113 moves closer to R111. The change is caused by a rearrangement of L2(B6).

Materials and Methods

MD simulations were performed using Gromacs-5.1.[3823] The NMR structure of PLAAT3 (2KYT) [41] and PLAAT4 (2MY9) [42] were selected for the simulations as starting structures and topology files were created from them. The AMBER ff99sb-ILDN force-field provided with GROMACS was used.[43] The models were then solvated in a periodic water box of 1 nm and 2 nm cubic edge length for (PLAAT3) and (PLAAT4), respectively. The latter is larger due to the elongated conformation of the protein. The TIP3P water model was used.[44,45] Three Na^+ counterions were automatically placed by the GROMACS program throughout the water box such that the final system had net zero charge. After solvation and neutralization, the systems were energy minimized by 5000 steps of minimization using the steepest descent algorithm. Minimized systems were further equilibrated under NVT and NPT conditions for 500 ps with a step size of 2 fs using position restraints on the protein and a temperature of 300 K and 1 atm. pressure controlled by the velocity rescaling (modified Berendsen) thermostat[46] and Parrinello-Rahman barostat.[47] The equilibrated systems were finally subjected to a 100 ns simulation run under NPT without any position restraints, and coordinates were saved after every ps. Two simulations were carried out with different starting seeds for both PLAAT3 and PLAAT4 where each seed represents a simulation at a different velocity. The trajectories were analysed using the inbuilt modules available in the GROMACS suite and visualized by means of the VMD[48]/Chimera [49] program.

Principal component analysis was carried out by first building the covariance matrix of atomic fluctuations and then generating a set of eigenvectors and eigenvalues by the diagonalization of the covariance matrix. The two eigenvectors that corresponded to the two largest eigenvalues were chosen as the principal components describing most of the collective motions or essential dynamics. The residues involved in these two largest eigenvectors were extracted by using a cut-off of 2 Å RMS fluctuations of individual atoms described by the two eigenvectors using an in-house program. The motions of these residues were further analysed by observing the MD trajectory.

Supplementary Figures

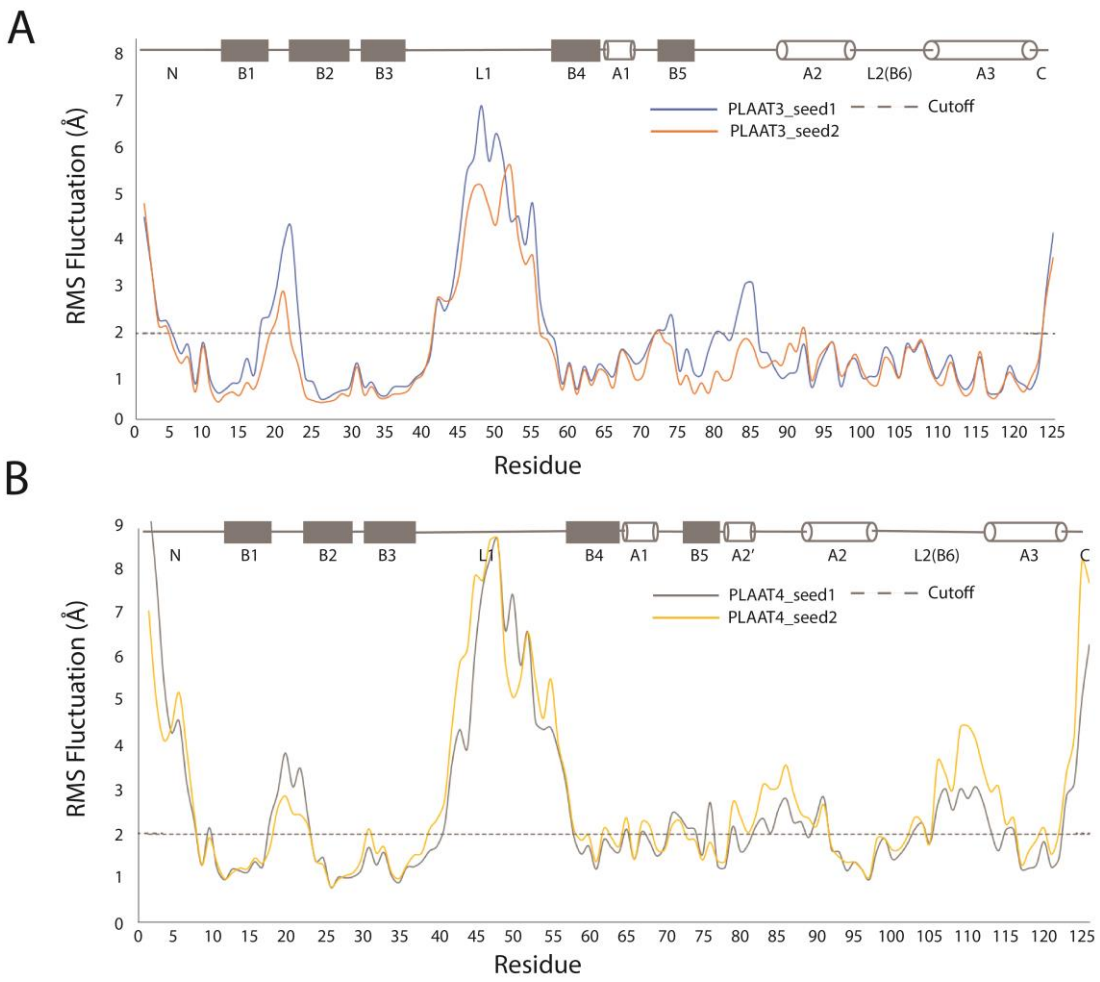

Figure S3.1 RMS fluctuations per residue. For each residue, the RMS fluctuations in the MD runs are plotted for PLAAT3 (A) and PLAAT4 (B). A cut-off of 2 Å is indicated with a dashed line. Secondary structure of the starting structure is indicated at the top and named as per Table 2.1.

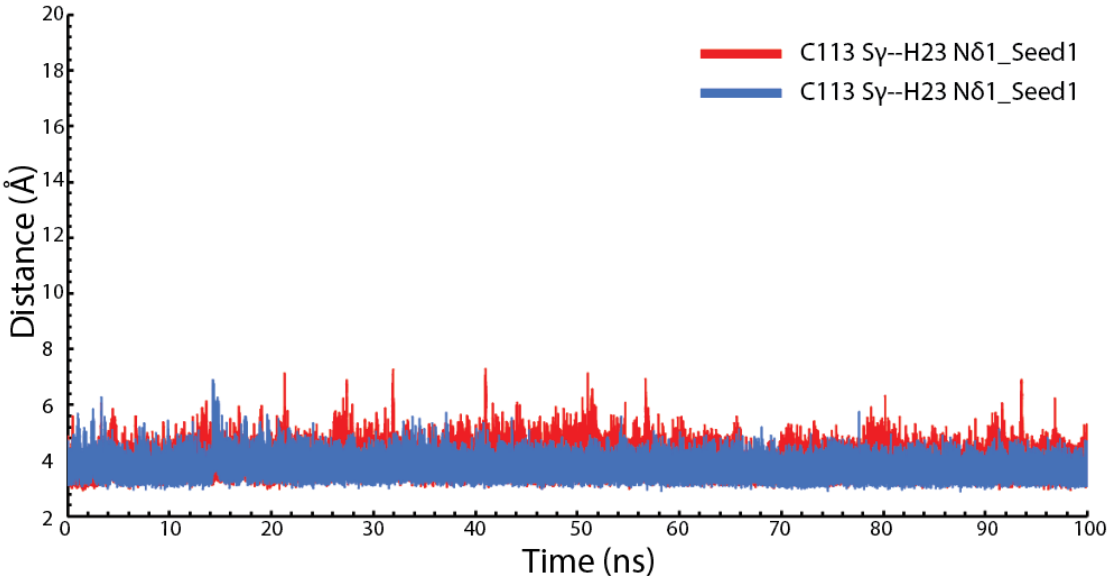

Figure S3.2 Inter-residue heavy atom distances during the two runs of MD simulations (seed 1 and seed 2). In PLAAT3, the distance between C113S_{γ} and H23$N_{\delta 1}$ is maintained throughout the two runs of simulations, suggesting that the catalytic triad is maintained.

References

(1) Chu, Y.-P., Chang, C.-H., Shiu, J.-H., Chang, Y.-T., Chen, C.-Y., and Chuang, W.-J. (2011) Solution structure and backbone dynamics of the DNA-binding domain of FOXP1: insight into its domain swapping and DNA binding. *Protein Sci. 20*, 908–924.

(2) Moorman, V. R., Valentine, K. G., Bédard, S., Kasinath, V., Dogan, J., Love, F. M., and Wand, A. J. (2014) Dynamic and thermodynamic response of the Ras protein Cdc42Hs upon association with the effector domain of PAK3. *J. Mol. Biol. 426*, 3520–3538.

(3) Guenneugues, M., Gilquin, B., Wolff, N., Ménez, A., and Zinn-Justin, S. (1999) Internal motion time scales of a small, highly stable and disulfide-rich protein: A 15N, 13C NMR and molecular dynamics study. *J. Biomol. NMR 14*, 47–66.

(4) Chua, C. E. L., and Tang, B. L. (2015) The role of the small GTPase Rab31 in cancer. *J. Cell. Mol. Med. 19*, 1–10.

(5) Ma, L., Sham, Y. Y., Walters, K. J., and Towle, H. C. (2007) A critical role for the loop region of the basic helix-loop-helix/leucine zipper protein Mlx in DNA binding and glucose-regulated transcription. *Nucleic Acids Res. 35*, 35–44.

(6) Sunada, S., and Go, N. (1996) Calculation of nuclear magnetic resonance order parameters in proteins by normal mode analysis. II. Contribution from localized high frequency motions. *J. Chem. Phys. 105*, 6560–6564.

(7) Gu, Y., Li, D.-W., and Brüschweiler, R. (2014) NMR order parameter determination from long molecular dynamics trajectories for objective comparison with experiment. *J. Chem. Theory Comput. 10*, 2599–2607.

(8) Chalmers, G., Glushka, J. N., Foley, B. L., Woods, R. J., and Prestegard, J. H. (2016) Direct NOE simulation from long MD trajectories. *J. Magn. Reson. 265*, 1–9.

(9) Tolman, J. R., Al-Hashimi, H. M., Kay, L. E., and Prestegard, J. H. (2001) Structural and dynamic analysis of residual dipolar coupling data for proteins. *J. Am. Chem. Soc. 123*, 1416–1424.

(10) McCammon, J. A., Gelin, B. R., and Karplus, M. (1977) Dynamics of folded proteins. *Nature 267*, 585.

(11) Krepl, M., Cléry, A., Blatter, M., Allain, F. H. T., and Sponer, J. (2016) Synergy between NMR measurements and MD simulations of protein/RNA complexes: application to the RRMs, the most common RNA recognition motifs. *Nucleic Acids Res. 44*, 6452–6470.

(12) Phillips, J. C., Braun, R., Wang, W., Gumbart, J., Tajkhorshid, E., Villa, E., Chipot, C., Skeel, R. D., Kalé, L., and Schulten, K. (2005) Scalable molecular dynamics with NAMD. *J. Comput. Chem. 26*, 1781–1802.

(13) Pronk, S., Páll, S., Schulz, R., Larsson, P., Bjelkmar, P., Apostolov, R., Shirts, M. R., Smith, J. C., Kasson, P. M., van der Spoel, D., Hess, B., and Lindahl, E. (2013) GROMACS 4.5: a high-throughput and highly parallel open source molecular simulation toolkit. *Bioinformatics 29*, 845–854.
(14) Case, D. A., Cheatham 3rd, T. E., Darden, T., Gohlke, H., Luo, R., Merz Jr, K. M., Onufriev, A., Simmerling, C., Wang, B., and Woods, R. J. (2005) The Amber biomolecular simulation programs. *J. Comput. Chem. 26*, 1668–1688.
(15) Dror, R. O., Dirks, R. M., Grossman, J. P., Xu, H., and Shaw, D. E. (2012) Biomolecular simulation: a computational microscope for molecular biology. *Annu. Rev. Biophys. 41*, 429–452.
(16) Foloppe, N., and MacKerell Alexander D., J. (2000) All-atom empirical force field for nucleic acids: I. Parameter optimization based on small molecule and condensed phase macromolecular target data. *J. Comput. Chem. 21*, 86–104.
(17) Duan, Y., Wu, C., Chowdhury, S., Lee, M. C., Xiong, G., Zhang, W., Yang, R., Cieplak, P., Luo, R., Lee, T., Caldwell, J., Wang, J., and Kollman, P. (2003) A point-charge force field for molecular mechanics simulations of proteins based on condensed-phase quantum mechanical calculations. *J. Comput. Chem. 24*, 1999–2012.
(18) Cornell, W. D., Cieplak, P., Bayly, C. I., Gould, I. R., Merz, K. M., Ferguson, D. M., Spellmeyer, D. C., Fox, T., Caldwell, J. W., and Kollman, P. A. (1995) A second generation force field for the simulation of proteins, nucleic acids, and organic molecules. *J. Am. Chem. Soc. 117*, 5179–5197.
(19) Kollman, P. A. (1996) Advances and continuing challenges in achieving realistic and predictive simulations of the properties of organic and biological molecules. *Acc. Chem. Res. 29*, 461–469.
(20) Oostenbrink, C., Villa, A., Mark, A. E., and Van Gunsteren, W. F. (2004) A biomolecular force field based on the free enthalpy of hydration and solvation: The GROMOS force-field parameter sets 53A5 and 53A6. *J. Comput. Chem. 25*, 1656–1676.
(21) Schuler, L. D., Daura, X., and van Gunsteren, W. F. (2001) An improved GROMOS96 force field for aliphatic hydrocarbons in the condensed phase. *J. Comput. Chem. 22*, 1205–1218.
(22) Brooks, B. R., Brooks 3rd, C. L., Mackerell Jr, A. D., Nilsson, L., Petrella, R. J., Roux, B., Won, Y., Archontis, G., Bartels, C., Boresch, S., Caflisch, A., Caves, L., Cui, Q., Dinner, A. R., Feig, M., Fischer, S., Gao, J., Hodoscek, M., Im, W., Kuczera, K., Lazaridis, T., Ma, J., Ovchinnikov, V., Paci, E., Pastor, R. W., Post, C. B., Pu, J. Z., Schaefer, M., Tidor, B.,

Venable, R. M., Woodcock, H. L., Wu, X., Yang, W., York, D. M., and Karplus, M. (2009) CHARMM: the biomolecular simulation program. *J. Comput. Chem. 30*, 1545–1614.
(23) Hess, B., Kutzner, C., van der Spoel, D., and Lindahl, E. (2008) GROMACS 4: algorithms for highly efficient, load-balanced, and scalable molecular simulation. *J. Chem. Theory Comput. 4*, 435–447.
(24) Roux, B., and Simonson, T. (1999) Implicit solvent models. *Biophys. Chem. 78*, 1–20.
(25) Jorgensen, W. L., Chandrasekhar, J., Madura, J. D., Impey, R. W., and Klein, M. L. (1983) Comparison of simple potential functions for simulating liquid water. *J. Chem. Phys. 79*, 926–935.
(26) Mahoney, M. W., and Jorgensen, W. L. (2000) A five-site model for liquid water and the reproduction of the density anomaly by rigid, nonpolarizable potential functions. *J. Chem. Phys. 112*, 8910–8922.
(27) Berendsen, H. J. C., Grigera, J. R., and Straatsma, T. P. (1987) The missing term in effective pair potentials. *J. Phys. Chem. 91*, 6269–6271.
(28) Shao, J., Tanner, S. W., Thompson, N., and Cheatham, T. E. (2007) Clustering molecular dynamics trajectories: 1. characterizing the performance of different clustering algorithms. *J. Chem. Theory Comput. 3*, 2312–2334.
(29) Karpen, M. E., Tobias, D. J., and Brooks, C. L. (1993) Statistical clustering techniques for the analysis of long molecular dynamics trajectories: analysis of 2.2-ns trajectories of YPGDV. *Biochemistry 32*, 412–420.
(30) Shenkin, P. S., and McDonald, D. Q. (2018) Cluster analysis of molecular conformations. *J. Comput. Chem. 15*, 899–916.
(31) David, C. C., and Jacobs, D. J. (2014) Principal component analysis: a method for determining the essential dynamics of proteins. *Methods Mol. Biol. 1084*, 193–226.
(32) Berendsen, H. J. C., and Hayward, S. (2000) Collective protein dynamics in relation to function. *Curr. Opin. Struct. Biol. 10*, 165–169.
(33) Amadei, A., Linssen, A. B. M., de Groot, B. L., van Aalten, D. M. F., and Berendsen, H. J. C. (1996) An efficient method for sampling the essential subspace of proteins. *J. Biomol. Struct. Dyn. 13*, 615–625.
(34) Amadei, A., Linssen, A. B. M., and Berendsen, H. J. C. (2018) Essential dynamics of proteins. *Proteins Struct. Funct. Bioinforma. 17*, 412–425.
(35) Salsbury, F. R., Crowder, M. W., Kingsmore, S. F., and Huntley, J. J. A. (2008) Molecular dynamic simulations of the metallo-beta-lactamase from Bacteroides fragilis in the presence and absence of a tight-binding inhibitor. *J. Mol. Model. 15*, 133.

(36) Wrabl, J. O., Shortle, D., and Woolf, T. B. (2000) Correlation between changes in nuclear magnetic resonance order parameters and conformational entropy: Molecular dynamics simulations of native and denatured staphylococcal nuclease. *Proteins Struct. Funct. Bioinforma. 38*, 123–133.
(37) Radkiewicz, J. L., and Brooks, C. L. (2000) Protein dynamics in enzymatic catalysis: exploration of dihydrofolate reductase. *J. Am. Chem. Soc. 122*, 225–231.
(38) Van Der Spoel, D., Lindahl, E., Hess, B., Groenhof, G., Mark, A. E., and Berendsen, H. J. C. (2005) GROMACS: Fast, flexible, and free. *J. Comput. Chem. 26*, 1701–1718.
(39) Panja, A. S., Maiti, S., and Bandyopadhyay, B. (2020) Protein stability governed by its structural plasticity is inferred by physicochemical factors and salt bridges. *Sci. Rep. 10*, 1822.
(40) Mamonova, T. B., Glyakina, A. V, Galzitskaya, O. V, and Kurnikova, M. G. (2013) Stability and rigidity/flexibility—Two sides of the same coin? *Biochim. Biophys. Acta - Proteins Proteomics 1834*, 854–866.
(41) Ren, X., Lin, J., Jin, C., and Xia, B. (2010) Solution structure of the N-terminal catalytic domain of human H-REV107--a novel circular permutated NlpC/P60 domain. *FEBS Lett. 584*, 4222–4226.
(42) Wei, H., Wang, L., Ren, X., Yu, W., Lin, J., Jin, C., and Xia, B. (2015) Structural and functional characterization of tumor suppressors TIG3 and H-REV107. *FEBS Lett. 589*, 1179–1186.
(43) Lindorff-Larsen, K., Piana, S., Palmo, K., Maragakis, P., Klepeis, J. L., Dror, R. O., and Shaw, D. E. (2010) Improved side-chain torsion potentials for the Amber ff99SB protein force field. *Proteins 78*, 1950–1958.
(44) Jorgensen, W. L. (1981) Quantum and statistical mechanical studies of liquids. 10. Transferable intermolecular potential functions for water, alcohols, and ethers. Application to liquid water. *J. Am. Chem. Soc. 103*, 335–340.
(45) Mark, P., and Nilsson, L. (2001) Structure and dynamics of the TIP3P, SPC, and SPC/E water models at 298 K. *J. Phys. Chem. A 105*, 9954–9960.
(46) Bussi, G., Donadio, D., and Parrinello, M. (2007) Canonical sampling through velocity rescaling. *J. Chem. Phys. 126*, 14101.
(47) Parrinello, M., and Rahman, A. (1981) Polymorphic transitions in single crystals: A new molecular dynamics method. *J. Appl. Phys. 52*, 7182–7190.
(48) Humphrey, W., Dalke, A., and Schulten, K. (1996) VMD: Visual molecular dynamics. *J. Mol. Graph. 14*, 33–38.

(49) Pettersen, E. F., Goddard, T. D., Huang, C. C., Couch, G. S., Greenblatt, D. M., Meng, E. C., and Ferrin, T. E. (2004) UCSF Chimera—A visualization system for exploratory research and analysis. *J. Comput. Chem. 25*, 1605–1612.